Petalite postdating spodumene in pegmatite as a consequence of the ~2.02 Ga meteorite impact in the Vredefort structure, southern Africa

H.M. Rajesh [a,*], M.W. Knoper [b], G.A. Belyanin [b], O.G. Safonov [c,d,b], C. Schmidt [e]

[a] *Department of Earth and Environmental Sciences, BIUST, Botswana*
[b] *Department of Geology, University of Johannesburg, South Africa*
[c] *Korzhinskii Institute of Experimental Mineralogy RAS, Chernogolovka, Russia*
[d] *Department of Petrology and Volcanology, Geological Faculty, Moscow State University, Russia*
[e] *GFZ German Research Centre for Geosciences, Potsdam, Germany*

ARTICLE INFO

ABSTRACT

Rare-element granitic pegmatites enriched in lithium are economically important hosts for the lithium alumino-silicates, spodumene and petalite. Most spodumene and petalite crystallize from the pegmatite melt, depending on pressure and temperature. This paper reports the rare occurrence of petalite postdating the subsolidus stage in spodumene pegmatites within the ~2.02 Ga Vredefort impact structure, the largest, oldest and most deeply eroded meteorite impact structure currently known on Earth. The studied spodumene-bearing pegmatites post-date the deformation fabric in the surrounding amphibolites of the granitoid-greenstone terrane. Impact-related veins of fragment-rich pseudotachylites cut across the pegmatites. Spodumene, albite and quartz constitute the primary mineral assemblage of the pegmatites. Muscovite is late magmatic and contains inclusions of spodumene and albite. During the subsolidus stage, K-feldspar replaced spodumene and albite during pervasive meta-somatic alteration. Samples collected closer to the pseudotachylites show reaction textures between spodumene and quartz without the involvement of muscovite. Raman spectroscopy and microprobe analyses show that the reaction textures consist of quartz and petalite. Unlike spodumene, petalite does not show a replacement by K-feldspar. The $^{40}Ar/^{39}Ar$ muscovite age of 2027 ± 8 Ma coincides with the timing of the meteorite impact and documents its effect on the spodumene pegmatites. We suggest that the formation of petalite after spodumene was related to heating, which was generated in the target rocks by the post-shock thermal event. Thus, the unique conditions associated with the meteorite impact can not only result in the formation of rare minerals in the target rocks, but can also account for rare scenarios resulting in phases that would not otherwise form in nature.

© 2020 Elsevier B.V. All rights reserved.

1. Introduction

Spodumene-bearing granitic pegmatites (spodumene pegmatites hereafter) are the most common lithium-rich rare-element pegmatites (Černý, 1991; Černý and Ercit, 2005; London, 2008). Petalite-bearing granitic pegmatites are also common (Chakoumakos and Lumpkin, 1990; Stewart, 1978). Phase relations in the system $LiAlSiO_4$-SiO_2-H_2O are very sensitive to variations in pressure (P) and temperature (T) (Fig. 1; Stewart, 1978; London, 1984; Krivovichev, 2004). The primary magmatic phases, spodumene ($LiAlSi_2O_6$) and petalite ($LiAlSi_4O_{10}$), are antithetic in terms of P and T, so that petalite is the high-T – low-P equivalent of spodumene in lithium-rich pegmatites (Krivovichev, 2004; London, 1984; Stewart, 1978). During the late

stage of evolution of granitic pegmatites, residual fluids modify the original composition of primary mineral phases. Eucryptite ($LiAlSiO_4$), which is stable at low P and T (Fig. 1), is a secondary mineral replacing petalite and/or spodumene in lithium-rich pegmatites. Other common alteration phases include albite, K-feldspar, mica and clay minerals (Lagache et al., 1995; London and Burt, 1982; Wood and Williams-Jones, 1993). As the spodumene-petalite transition typically occurs under magmatic conditions, formation of petalite in the subsolidus is less likely in a lithium-rich pegmatite.

Within the Kaapvaal craton in southern Africa, spodumene pegmatites occur in a unique setting – within the Vredefort meteorite impact structure (Fig. 2a). This paper focuses on these pegmatites. The main aim of the study is to demonstrate that the pegmatite mineral assemblages and textures are uniquely the product of the post-shock thermal event and/or decompression as a consequence of the Vredefort meteorite impact at ~2.02 Ga. The results have implications for the study of rare

---

* Corresponding author.
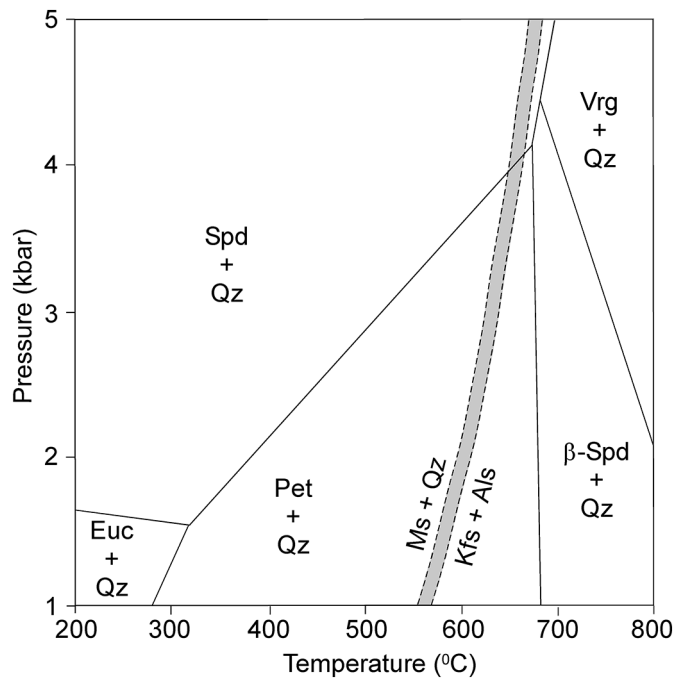*E-mail address:* rajesh.hm@biust.ac.bw (H.M. Rajesh).

Fig. 1. Pressure-temperature diagram showing phase boundaries of the system LiAlSiO$_4$-SiO$_2$-H$_2$O [from London, 1984]. Equilibria curves showing the break-down of muscovite + quartz (muscovite + quartz = K-feldspar + Al$_2$SiO$_5$ + H$_2$O) from Kerrick (1972) is also shown. Spd – spodumene; Vrg – virgilite; Euc – eucryptite; Pet – petalite; Qz – quartz; Ms – muscovite; Als – aluminosilicate.

minerals formed under unique scenarios in target rocks within meteorite impact structures.

2. Geological setting

The studied spodumene pegmatites occur in the southeastern sector of the 2023 ± 4 Ma (U—Pb zircon; Kamo et al., 1996) Vredefort impact structure, in an inlier dominated by granitoid-greenstone rocks (Fig. 2a, b). The 90 km wide eroded remnant of the original ~250 km Vredefort impact structure consists of an uplifted central core of predominantly high-grade Mesoarchean granitoid-greenstone rocks, exposing a section of the middle and, possibly, lower crust. It is surrounded by a collar of upturned Neoarchean to Paleoproterozoic supracrustal strata (Witwatersrand, Ventersdorp and Transvaal Supergroups) that unconformably overlie the basement rocks (Fig. 2b; Gibson and Reimold, 2008). A number of ultramafic, mafic, intermediate and felsic intrusive bodies related to the ~2.06–2.05 Ga Bushveld Complex (Fig. 2a) magmatic event occur in the northern collar of the Vredefort structure (Bisschoff, 1972; Coetzee et al., 2006; De Waal et al., 2006, 2008; Graham et al., 2005). One of the largest bodies is the 2052 ± 14 Ma Schurwedraai alkali granite, which intrudes the supracrustal rocks of the lower Witwatersrand Supergroup (Fig. 2b; Graham et al., 2005). Like other pre-impact rocks, the different *syn*-Bushveld intrusions are cut across by dark fragment-rich veins of pseudotachylites, related to the ~2.02 Ga impact event. Except for an inlier, the southeastern part of the impact structure is covered by the Phanerozoic Karoo Supergroup sediments (Fig. 2b; Antoine et al., 1990; Minnitt et al., 1994; Lana et al., 2003; Hart et al., 2004).

The inlier in the southeastern sector, termed the Greenlands granitoid-greenstone complex, consists dominantly of ultramafic to mafic metavolcanics intercalated with subordinate banded iron formations and felsic schists (Fig. 3). The greenstone rocks have been dated at ~3.30 Ga (actinolite-chlorite schist; Reimold et al., 1988; Lana et al.,

2003). In the northern part, the greenstone rocks are bounded by migmatitic granitoid gneisses and amphibolites. Available age data bracket the migmatitic granitoid gneisses to ~3.11–2.97 Ga (Reimold et al., 1988; Robertson, 1988). The granitoid gneisses contain inclusions of amphibolites, and are locally pegmatitic, made up dominantly of quartz and plagioclase, together with mica and garnet. Gneissic rocks and amphibolites in the northern part display a strong northeast-trending fabric. This differs from the northwest-trending foliation observed in the greenstone rocks to the south (Fig. 3; Colliston and Reimold, 1990; Minnitt et al., 1994; Lana et al., 2003). The northeast-trending fabric forms part of the mylonitic Broodkop shear zone (Fig. 3), and represents the contact between the greenstone rocks and higher-grade gneisses (Colliston and Reimold, 1990; Lana et al., 2003, 2006).

The deformed and/or metamorphosed granitoid-greenstone rocks in the Greenlands region are intruded by several pre-impact sheet-like gabbroic bodies of tholeiitic affinity (Fig. 3; Pybus, 1995; Reimold et al., 2000; Lana et al., 2003). Similar mafic intrusions occurring in the northern collar of the Vredefort impact structure are related to the ~2.7 Ga Ventersdorp magmatism (Pybus, 1995). Unlike the pre-impact intrusions, which are cut across by pseudotachylite veins (Reimold and Colliston, 1994), the post-impact intrusions in the Greenlands region are characterized by undeformed tholeiitic gabbroic intrusions (Fig. 3). Available geochronologic data relate these mafic intrusions to the ~1.1 Ga Anna's Rust Sheet event (Fig. 2b; Reimold et al., 2000), which occurs in both the core and collar regions of the Vredefort structure and are not cross-cut by pseudotachylite veins.

3. Field relations of the spodumene pegmatites

Spodumene pegmatites occur as isolated bodies within amphibolites or greenschist rocks (dominantly actinolite-chlorite schist; Figs. 3 and 4a, b). The contacts are not exposed (Fig. 4c, d). The pegmatite bodies show no deformation fabric and postdate a strong northeast-trending fabric in the surrounding amphibolites and northwest-trending fabric of the greenschist rocks (Fig. 4a to e). Bisschoff and Bisschoff (1988) documented the occurrence of holmquistite (lithium-dominant amphibole) replacing hornblende in the amphibolites. They suggested that the presence of a meter-wide metasomatic aureole within the host amphibolites was produced by the lithium-bearing fluids that emanated from the spodumene pegmatites. The samples for the present study were collected from the spodumene pegmatites in the amphibolites.

The pegmatite is a coarse-grained, plagioclase and quartz dominated rock with zones rich in lath-shaped randomly oriented spodumene crystals (length: ~1 to 15 cms; width: ~1 to 5 cms; Fig. 4e to g). Locally, they exhibit a preferential orientation subperpendicular to the margin of the pegmatite sheets (Fig. 4h). No zoning is present in the pegmatite. Minor aplitic veins cut across the pegmatite (Fig. 4i). Weathered exposures are pale ash-brown in color, imparted by feldspar and spodumene crystals, with white quartz standing out (Fig. 4g to i). Dark fragment-rich centimeter-scale pseudotachylite veins related to the ~2.02 Ga meteorite impact cut across the spodumene pegmatites (Fig. 5a to c). The fragments are dominantly quartz and plagioclase from the host pegmatite. Fragments along the center of pseudotachylite veins have rounded boundaries, whereas those near the margins are sub-angular with the angular side facing the margin (Fig. 5d, e). The rounded fragments in the center of spodumene pegmatite hosted pseudotachylite veins are irregularly distributed. This is in contrast to rounded fragments elongated parallel to the length of granitoid hosted pseudotachylite veins (Fig. 5f) as often observed elsewhere in the Vredefort impact structure.

3.1. Timing of the spodumene pegmatites

The northeast-trending mylonitic fabric within the Broodkop shear zone affected the amphibolites and not the spodumene pegmatites which intrude the meta-basaltic rocks (Figs. 3 and 4a to e). Lana et al.
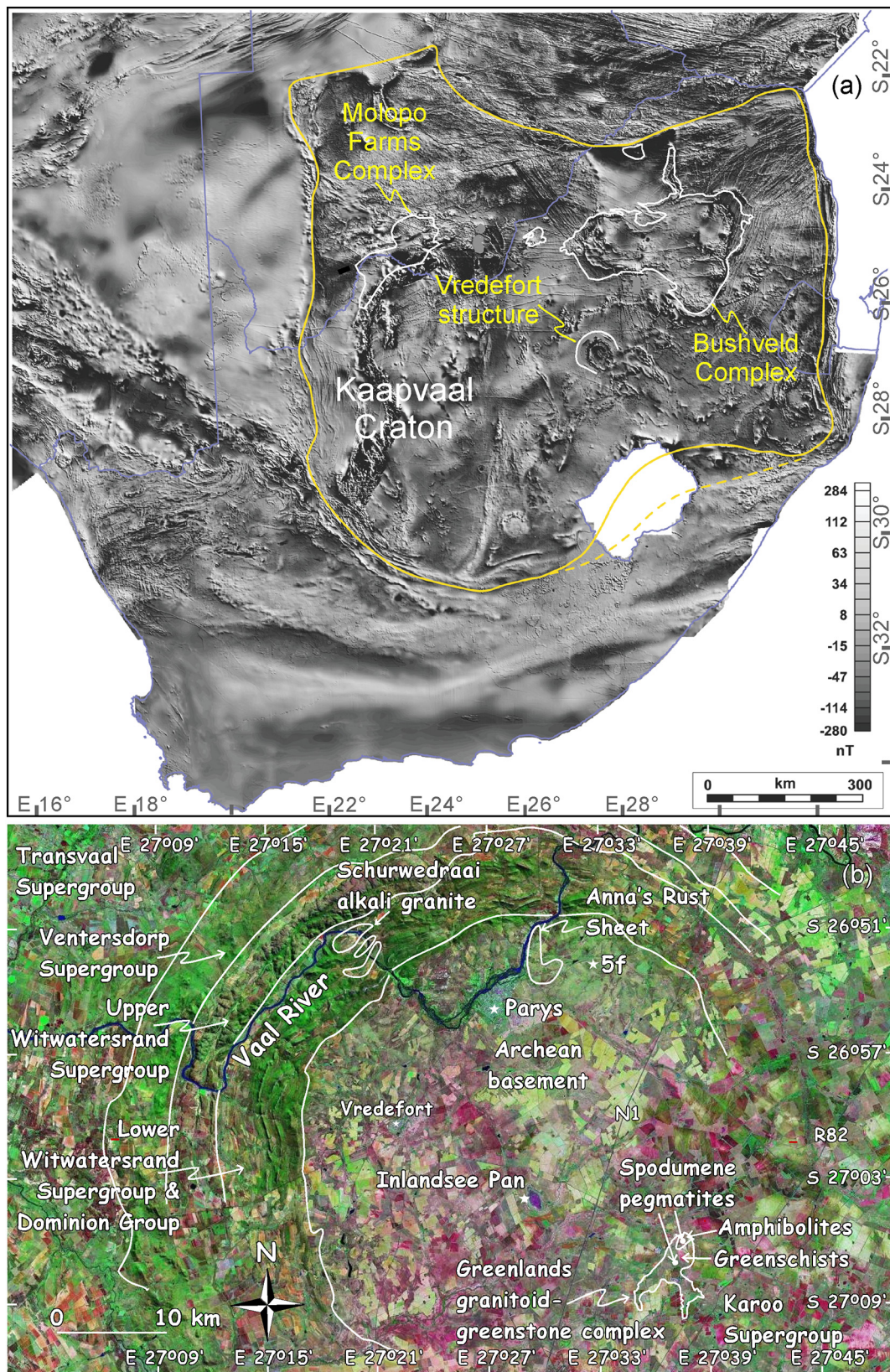
Fig. 2. (a) The known extent of Kaapvaal Craton (yellow line; allochthonous zone is dashed) shown on a total magnetic intensity (TMI) image of southern Africa (reproduced and modified after McCarthy et al., 2018). The ~2.06–2.05 Ga Bushveld Complex and Molopo Farms Complex layered intrusions, and the ~2.02 Ga Vredefort impact structure are indicated. **(b)** General geological map of the Vredefort impact structure shown on a Landsat TM742 satellite image. The location of spodumene pegmatite occurrences within metavolcanics rocks of the Greenlands granitoid-greenstone complex is shown. Outline of the different geologic units were derived from Gibson and Reimold (2008). (For interpretation of the references to color in this figure legend, the reader is referred to the web version of this article.)
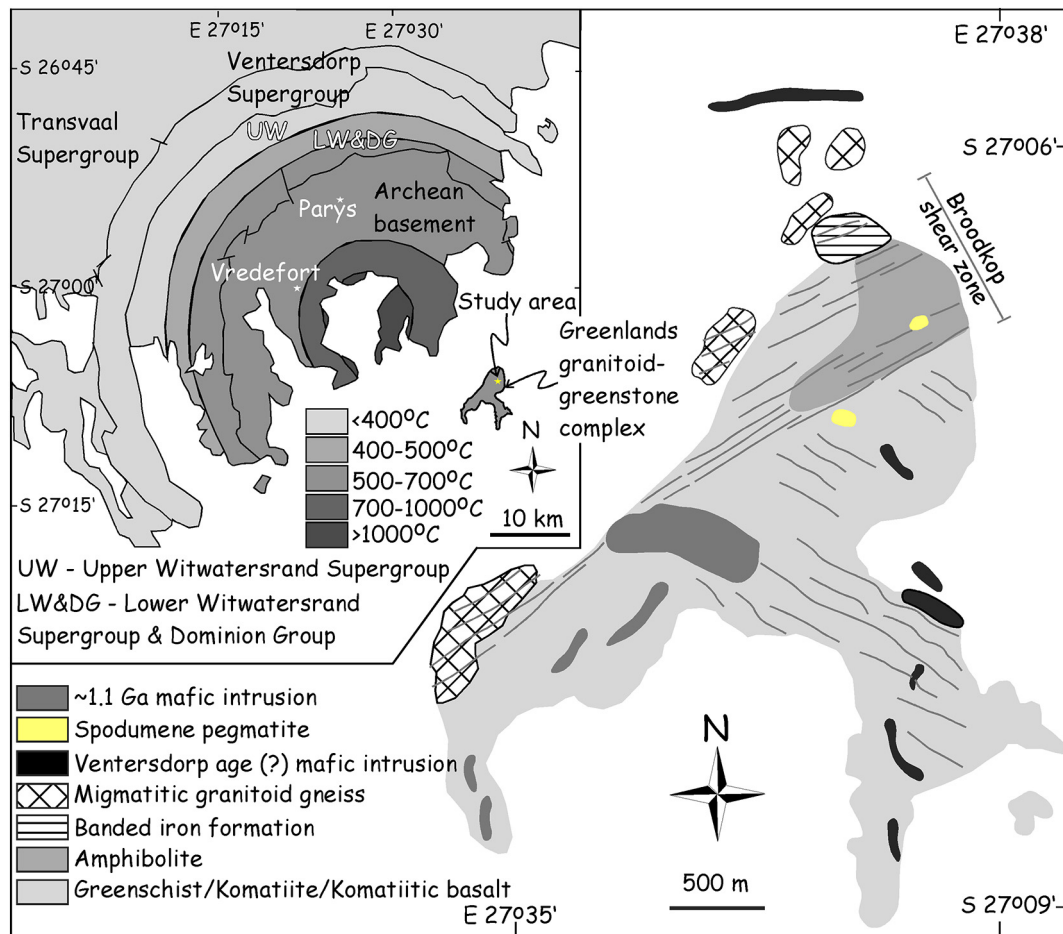
Fig. 3. Generalized geological map of the Greenlands granitoid-greenstone complex showing the spodumene pegmatite occurrences (from Lana et al., 2003). The grey lines indicate the northeast-trending fabric in amphibolites, banded iron formations and migmatitic granitoid gneiss, and northwest-trending fabric in greenschist rocks. Inset is a map of the Vredefort impact structure showing the post-shock temperature estimates based on metamorphic assemblages (from Gibson and Reimold, 2008). The Greenlands granitoid-greenstone complex occurs within the intermediate zone with post-shock temperature estimates of 500–700 °C. The outlines correspond with the different geological units in Fig. 2b.

(2006) pointed out that the Broodkop shear zone developed after the peak of high-grade metamorphism dated at ~3.08 Ga (Armstrong et al., 2006; Flowers et al., 2003; Hart et al., 1999; Moser et al., 2001). A suite of aplitic dykes that postdate the mylonitic fabric in migmatitic granitoid gneiss was dated at ~3.06 Ga (Armstrong et al., 2006). Thus, the Broodkop shear zone likely developed within the period ~3.08–3.06 Ga (Lana et al., 2006). Taking into account of the ~2.02 Ga age for pseudotachylite veins (Kamo et al., 1996), the timing of the spodumene pegmatites should be constrained to ~3.06–2.02 Ga. In contrast, Moser et al. (2011) presented an ID-TIMS zircon age of 1136 ± 47 Ma for the spodumene pegmatites. However, the field relations of the ~2.02 Ga pseudotachylite veins crosscutting the spodumene pegmatites (Fig. 5) clearly indicate a pre-impact age for the pegmatites, and the age obtained by Moser et al. (2011) is likely a Pb-loss event (see Rajesh and Knoper, 2012). The spodumene pegmatite sample dated by Moser et al. (2011) seemed to be collected in the region south of the Broodkop shear zone where low-grade metavolcanics have been affected by post-impact mafic intrusions related to the ~1.1 Ga Anna's Rust Sheet event (Fig. 3).

4. Analytical methods

Samples were collected from the pegmatite bodies proximal as well as distal to the pseudotachylite veins. After detailed petrographic study using back-scattered electron (BSE) imaging, mineral chemical analyses were obtained using electron microprobe (EPMA). Energy dispersive

spectrometry (EDS) elemental mapping using scanning electron microscopy (SEM) was carried-out on textural domains. Raman spectroscopic analyses were carried-out on spodumene, quartz and Li-bearing reaction zones. In view of the effect of meteorite impact on the spodumene pegmatites, $^{40}Ar/^{39}Ar$ dating was carried-out on muscovite separated from the pegmatite. Analytical details are given in supplementary online material DR1.

5. Petrography

Large spodumene crystals are associated with albite and quartz (Fig. 6a, b). Spodumene and albite are extensively replaced by K-feldspar (spodumene more than albite; Fig. 6a to d). Muscovite form small flakes along spodumene grain margins or large flakes in the matrix (Fig. 6a to e). They show irregular lobate margins with spodumene and albite (Fig. 6a to d). Subhedral to euhedral spodumene and albite inclusions occur in muscovite (Fig. 6f to h). Rare inclusions of spodumene in muscovite do not exhibit any replacement texture (Fig. 6f, h). The above textural relations in the spodumene pegmatite indicate the late magmatic origin of muscovite. Mn-rich garnet occur in the matrix as well as inclusions in albite, mica and spodumene. Accessory minerals are apatite, sicklerite, columbite-tantalite and topaz. The likely impact-related microstructures in the pegmatite include bent twin lamellae in albite, undulose extinction in quartz, and deformed muscovite with local kink-like zones (see arrows in Fig. 6a to d and f to h, including insets). Fracturing seems to accompany the deformation structures.

Fig. 4. Field relations between the spodumene pegmatite and surrounding rocks from the Greenlands granitoid-greenstone complex. **(a)** Amphibolite. **(b)** Dominant greenschist (chlorite schist). **(c)** The contact between amphibolite and pegmatite. **(d)** Typical occurrence of the pegmatite. The undeformed pegmatites postdate the deformation fabric in the surrounding amphibolites. **(e to g)** Fresh (e, f) and weathered (g) pegmatite exposures with randomly oriented spodumene laths. **(h)** Spodumene crystals locally exhibit a preferred orientation subperpendicular (see inset) to the margin of the pegmatite sheets. **(i)** Minor aplitic veins cut across the pegmatite.

Fig. 5. Field photographs illustrating the relation between pseudotachylite veins related to the ~2.02 Ga meteorite impact and the pegmatite bodies. Fresh **(a)** and weathered **(b, c)** exposures with dark veins of fragment-rich pseudotachylites cutting across pegmatites. **(d, e)** Close-up of portions of the pseudotachylite vein in (c) illustrating the nature and distribution of the quartz and plagioclase fragments, broken out from the host pegmatite. The fragments occurring along the center of pseudotachylite veins have rounded margins, whereas those near the margins are sub-angular with the angular side facing the margin. **(f)** Pseudotachylite cutting across granitoid gneiss from the northeastern sector of the Vredefort impact structure (locality indicated as 5f in Fig. 2b). Note the rounded fragments elongated parallel to the length of the pseudotachylite. This contrasts with the irregular distribution of fragments in the pegmatite hosted pseudotachylite veins.

Samples collected closer to the pseudotachylite veins show a lithium-bearing phase surrounding spodumene in association with quartz. The width of the overgrowths commonly does not exceed ~10 μm, but in rare cases, it can be up to 25 μm. The common textural relation between the three phases are overgrowths of the lithium-bearing phase on quartz invading spodumene (Fig. 7a), spodumene inclusions in the lithium-bearing phase within quartz (Fig. 7b), and quartz inclusions with rims of the lithium-phase within spodumene (Fig. 7c). Rims of the lithium-phase on quartz can also occur with vermicular spodumene-quartz intergrowths (Fig. 7d). Significantly, the lithium-bearing phase is devoid of any of the subsolidus minerals that are common in spodumene (Fig. 7a to d). Muscovite and albite are associated with these textural domains. For example, the EDS elemental maps of a representative domain (Fig. 7e to h; elements Al, Si, K shown) show that the lithium-bearing phase overgrows inclusions of spodumene in quartz that have been partially replaced by muscovite. The rims of the lithium-bearing phase are continuous and occur not only at the interface between spodumene and quartz, but also between muscovite and quartz (Fig. 7e to h).
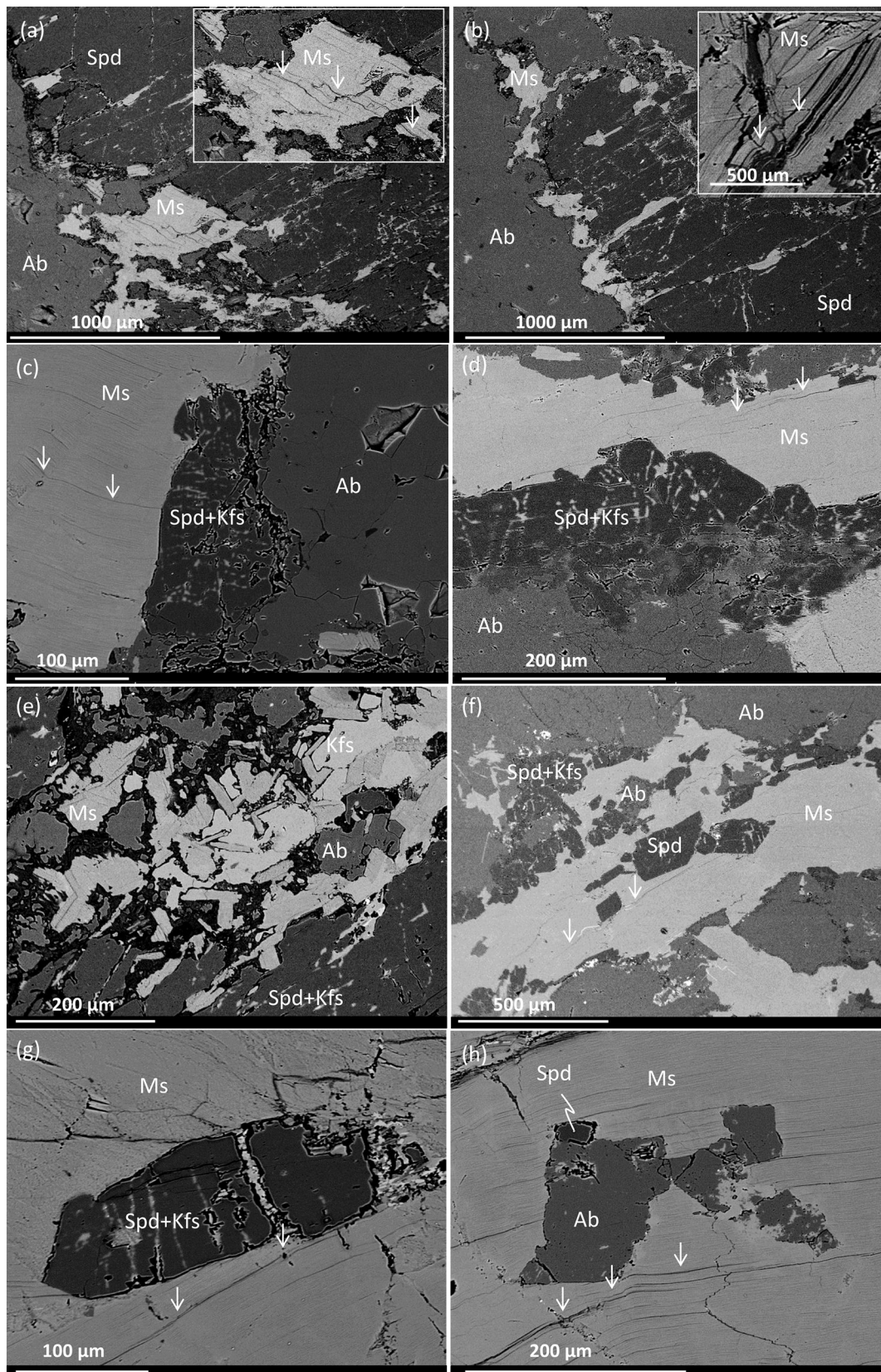
Fig. 6. BSE images illustrating the relation of spodumene (Spd), albite (Ab), muscovite (Ms) and K-feldspar (Kfs) in the spodumene pegmatites. **(a, b)** Muscovite occurs along the margin of large spodumene crystals. Insets in (a, b) illustrate deformed muscovite with local kink-like zones. **(c, d)** Spodumene is pervasively replaced by K-feldspar. Note the irregular lobate grain margins of spodumene, albite and muscovite. **(e)** Small crystals of muscovite and K-feldspar along the margin of spodumene. **(f)** Spodumene and albite inclusions in muscovite. Note the subhedral to euhedral outline of the inclusions. **(g)** Spodumene inclusion replaced by K-feldspar in muscovite. **(h)** Rare spodumene inclusions in muscovite exhibit no replacement textures involving K-feldspar. Arrows in the images point to microstructures preserved in muscovite that are likely related to impact-related deformation.
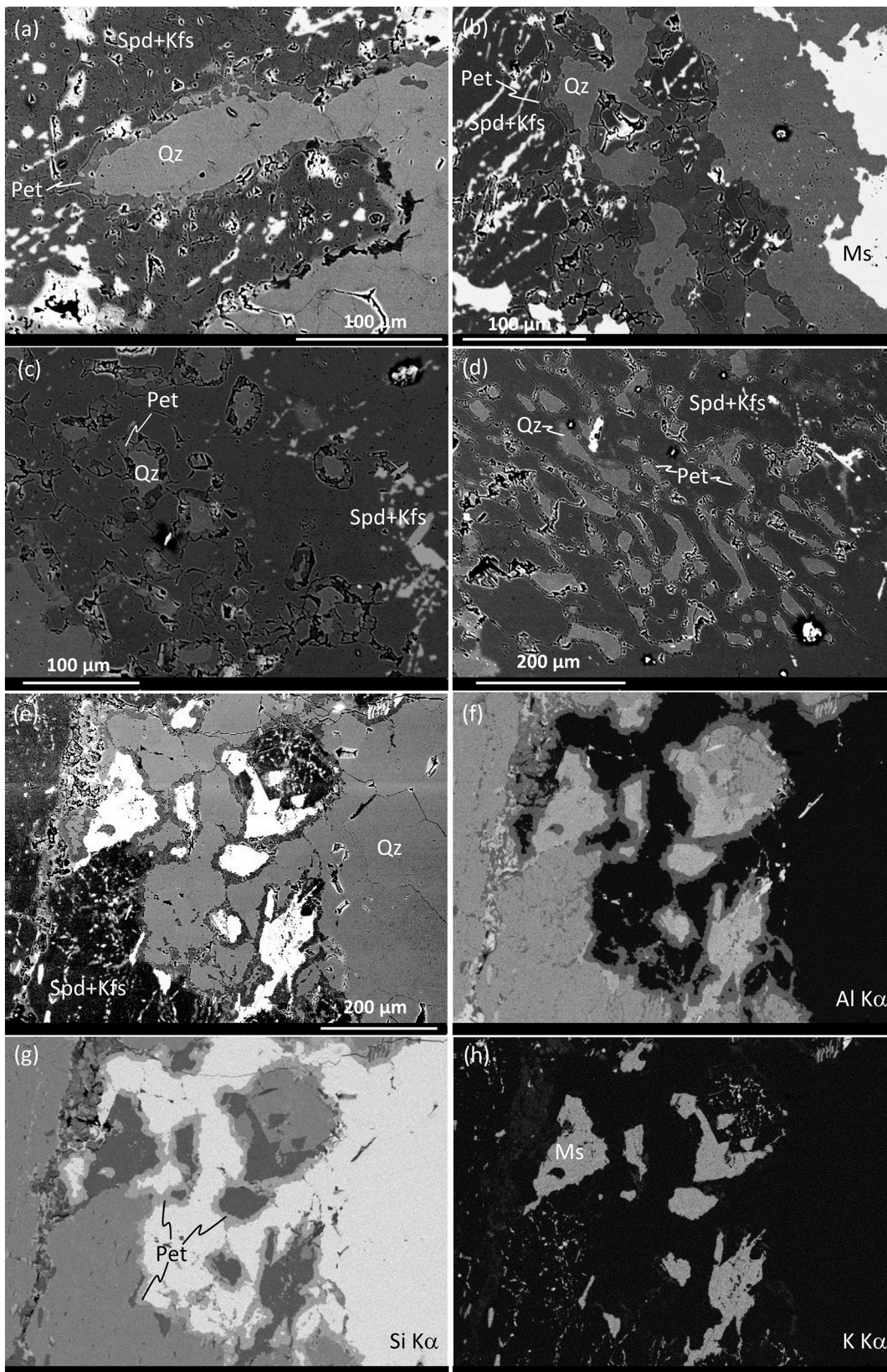
Fig. 7. BSE images **(a to e)** illustrating the textural relation between spodumene, quartz (Qz) and petalite (Pet) from the spodumene pegmatites. **(f to h)** EDS elemental mapping of a representative textural domain (e) is shown, with elements Al Kα (f), Si Kα (g) and K Kα (h) shown.

Table 1
Representative mineral chemical data of spodumene and petalite from the spodumene pegmatites.

	spodumene	spodumene	spodumene	spodumene	petalite	petalite	petalite	petalite
Na_2O	0.11	0.12	0.17	0.10	0.01	0.01	0.00	0.03
MgO	0.00	0.01	0.00	0.01	0.00	0.00	0.00	0.02
Al_2O_3	26.97	27.24	27.09	26.77	16.82	16.62	16.75	16.74
K_2O	0.01	0.00	0.00	0.00	0.02	0.01	0.00	0.01
SO_2	0.00	0.01	0.00	0.00	0.02	0.02	0.00	0.00
P_2O_5	0.00	0.00	0.00	0.00	0.02	0.00	0.01	0.01
SiO_2	64.54	63.75	64.30	64.68	78.29	78.04	78.31	78.05
CaO	0.00	0.02	0.00	0.00	0.02	0.00	0.00	0.00
BaO	0.00	0.00	0.01	0.00	0.06	0.05	0.00	0.11
TiO_2	0.00	0.04	0.02	0.01	0.00	0.03	0.03	0.00
FeO	0.59	0.75	0.68	0.80	0.00	0.05	0.00	0.00
MnO	0.20	0.06	0.08	0.01	0.00	0.01	0.00	0.02
Cr_2O_3	0.04	0.02	0.03	0.00	0.00	0.00	0.07	0.00
Li_2O	7.46	7.97	7.59	7.52	4.73	5.14	4.71	4.93
Total	99.91	99.99	99.97	99.91	99.98	99.99	99.87	99.91

6. Mineral chemistry

Chemical analyses of the overgrowth phase indicates a composition of lower aluminium (Al_2O_3 = ~16–17 wt%), alkalis (Na_2O + K_2O = ~0.01–0.04), iron (FeO = ~0.05 wt%), and lithium (Li_2O = ~5 wt%) content, than spodumene (Al_2O_3: ~26–27 wt%; Na_2O + K_2O = ~0.10–0.17 wt%; FeO = ~0.59–0.75 wt%; Li_2O = ~7–8 wt%) (Table 1). Two possible candidates of similar composition are petalite, which usually follows spodumene as a stable lithium aluminosilicate in lithium-rich pegmatites (e.g., Černý and Ferguson, 1972; Charoy et al., 2001), and virgilite ($Li_xAl_xSi_{3-x}O_6$), which has only been reported from the Macusani volcanic glass in Peru (French et al., 1978). In general, petalite

Table 2
Representative composition of muscovite from the spodumene pegmatites.

	Muscovite	Muscovite	Muscovite	Muscovite	Muscovite	Muscovite
SiO_2	46.18	45.28	45.26	45.81	46.13	45.52
TiO_2	0.02	0.01	0.00	0.03	0.02	0.04
Al_2O_3	34.80	33.43	32.92	32.77	32.73	34.83
FeO	2.60	2.57	2.97	3.26	2.58	2.33
MnO	0.19	0.15	0.23	0.16	0.20	0.15
MgO	0.33	0.39	0.30	0.29	0.29	0.24
CaO		0.01	0.02		0.05	
Na_2O	0.37	0.25	0.31	0.26	0.31	0.38
K_2O	9.47	9.16	9.44	9.63	8.98	10.06
ZnO	0.04	0.05	0.05	0.04	0.07	0.06
F	0.60	0.52	0.79	0.62	0.67	0.69
Cl	0.03		0.02			0.01
Cr_2O_3	0.02		0.01		0.01	0.00
Li_2O*	0.11	0.09	0.17	0.12	0.13	0.14
H_2O**	4.16	4.08	3.94	4.05	4.03	4.09
Subtotal	98.92	95.99	96.43	97.04	96.20	98.54
O=F,Cl	0.26	0.22	0.34	0.26	0.28	0.29
Total	98.66	95.77	96.10	96.78	95.92	98.25
O = 22						
Si	6.217	6.271	6.279	6.316	6.370	6.173
Al(IV)	1.783	1.729	1.721	1.684	1.630	1.827
Al(VI)	3.739	3.729	3.662	3.642	3.696	3.741
Ti	0.002	0.001		0.003	0.002	0.004
Cr	0.002		0.001		0.001	
Fe	0.293	0.298	0.345	0.376	0.298	0.264
Mn	0.022	0.018	0.027	0.019	0.023	0.017
Mg	0.066	0.081	0.062	0.060	0.060	0.049
Zn	0.004	0.005	0.005	0.004	0.007	0.006
Li*	0.060	0.048	0.095	0.065	0.074	0.076
Ca		0.001	0.003		0.007	
Na	0.097	0.067	0.083	0.070	0.083	0.100
K	1.626	1.618	1.670	1.694	1.582	1.740
OH**	3.738	3.772	3.649	3.730	3.707	3.702
F	0.255	0.228	0.347	0.270	0.293	0.296
Cl	0.007		0.005			0.002
TOTAL	17.910	17.866	17.953	17.932	17.833	17.997
X_{Mg}	0.18	0.21	0.15	0.14	0.17	0.16
Al_{total}	5.52	5.46	5.38	5.33	5.33	5.57

X_{Mg} = Mg/(Mg + Fe).
* **Li_2O calculation from** Monier and Robert (1986).
** **H_2O calculation after** Tindle and Webb (1990).

has slightly higher aluminium (Al$_2$O$_3$ = ~16.6–17.2 wt%) and lower lithium (Li$_2$O = ~4.4–4.8 wt%) concentrations than virgilite (Al$_2$O$_3$ = ~16–16.7 wt%; Li$_2$O = ~4.9–5 wt%) (Černý and Ferguson, 1972; French et al., 1978). On the other hand, iron content is low in petalite (FeO = ~0.03–0.05 wt%) in comparison to that reported for virgilite (FeO = ~0.59–1.65 wt%) (Černý and Ferguson, 1972; French et al., 1978). SEM-based qualitative spectrum analyses and mapping of Al and Si contents of adjacent spodumene and overgrowth domains from the studied samples indicated Al:Si ratios of 1:4, typical of petalite and different from that of virgilite.

Muscovite shows X$_{Mg}$ = Mg/(Mg + Fe) = 0.14–0.21, 0.001–0.004 apfu (atoms per formula unit) Ti, 5.33–5.57 apfu Al, 0.52–0.81 wt % F + Cl (Table 2). The low Li content (0.09–0.17 wt%) is not characteristic of lithian muscovites. However, in view of the overlapping nature of the parameters used to separate muscovite (mgli > −0.4; mgli <1.0; feal < −3.0; feal > −4.0) and lithian muscovite (mgli > −2.4; mgli < −0.4; feal < −3.0; feal > −3:8; mgli: Mg-Li; feal: Fe$_{tot}$ + Mn + Ti-Al^{vi}; Tischendorf et al., 1997), the possibility of the presence of lithian muscovite is not excluded.

7. Raman spectroscopy

Raman spectra were acquired on spodumene, quartz and the Li-bearing reaction zone, occurring in proximity. The spectra obtained for quartz from the studied sample shows diagnostic peaks at about 125, 206, and 463 cm^{-1} (Fig. 8a). Depending on orientation, spodumene from the studied sample exhibits the most intense Raman peaks at

about 248, 298, 355, 394, 522, 706, and 1072 cm^{-1} (Figs. 8b and 9). All of them are related to Si—O bending and Si—O stretching vibrations (Pommier et al., 2003; Stangarone et al., 2014).

The Raman spectrum of virgilite displays two characteristic overlapping bands at about 455 and 479 cm^{-1} and a weaker feature at about 790 cm^{-1} (see Benaway et al., 2012; Sirbescu et al., 2017). None of these bands were detected in the spectra of the reaction zones (Fig. 9). Raman spectra of the reaction zone yielded Raman bands for petalite and quartz even at a lateral resolution of 1 μm (Figs. 8c, d and 9). Raman bands at about 110, 146, 282, 321, and 492 cm^{-1} are only from petalite, which also has fairly intense peaks at about 355 and 385 cm^{-1} (Fig. 9). All of them are from Si—O bending and Si—O stretching modes, which are related to the folded [Si$_2$O$_5$]-layers linking to Li and Al tetrahedra (Tagai et al., 1982).

8. ^{40}Ar/^{39}Ar muscovite geochronology

The Ar analytical results for the studied muscovite, including Ca/K and Cl/K ratios, are listed in Table 3. The muscovite grain from the spodumene pegmatite yielded a plateau age of 2027 ± 8 Ma (Fig. 10). The Ca/K ratios of the muscovite is zero (Table 3). The closure temperature of the Ar—Ar isotopic system for the retention of radiogenic argon is about 425 °C for muscovite (Harrison et al., 2009). Any rise in the actual temperature which exceeds the closure temperature will likely result in complete resetting of the Ar—Ar isotopic system. Hence, the Ar—Ar age of muscovite likely represent
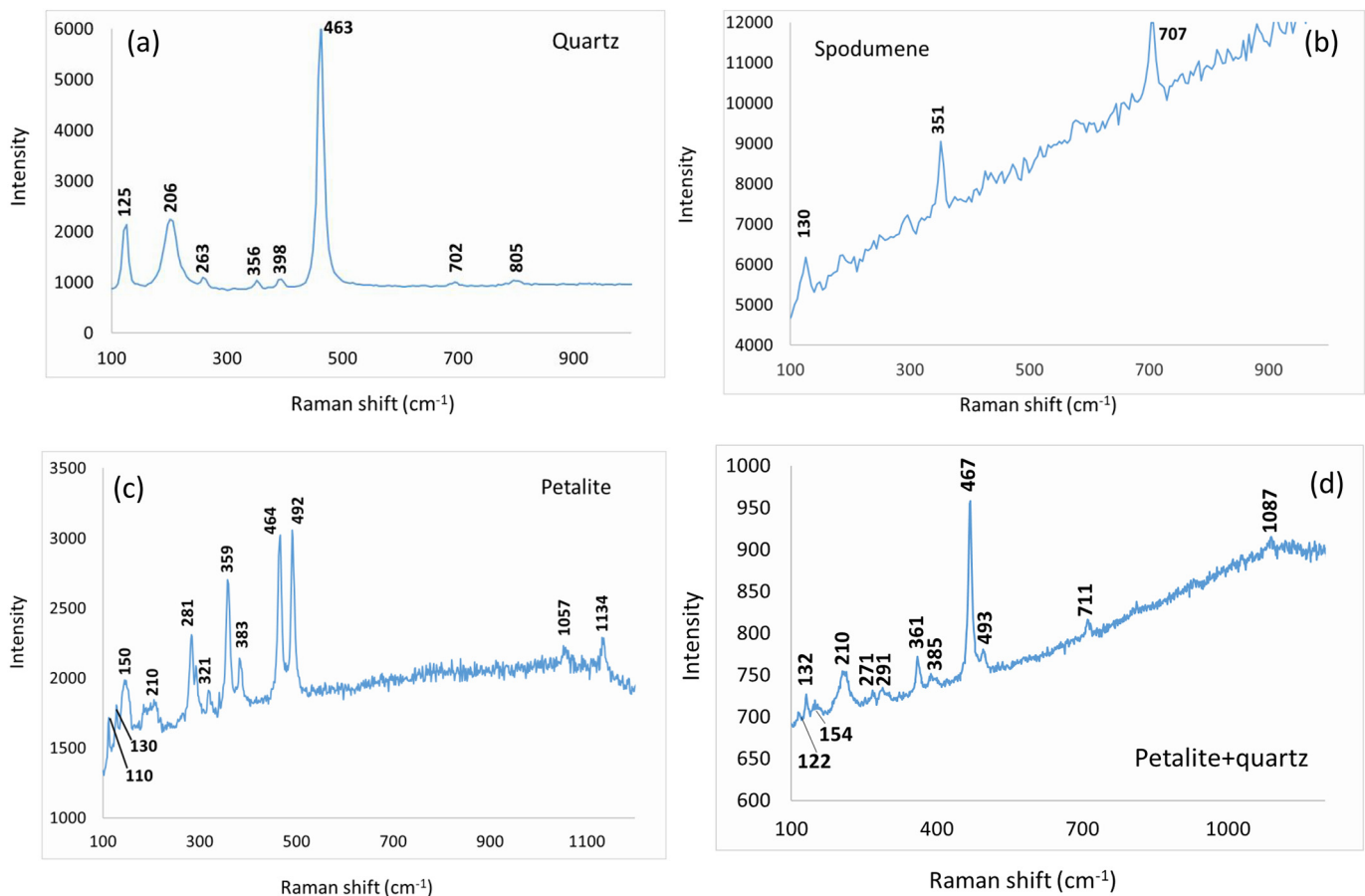

Fig. 8. Raman spectra of quartz (**a**), spodumene (**b**) and petalite + quartz (**c, d**).
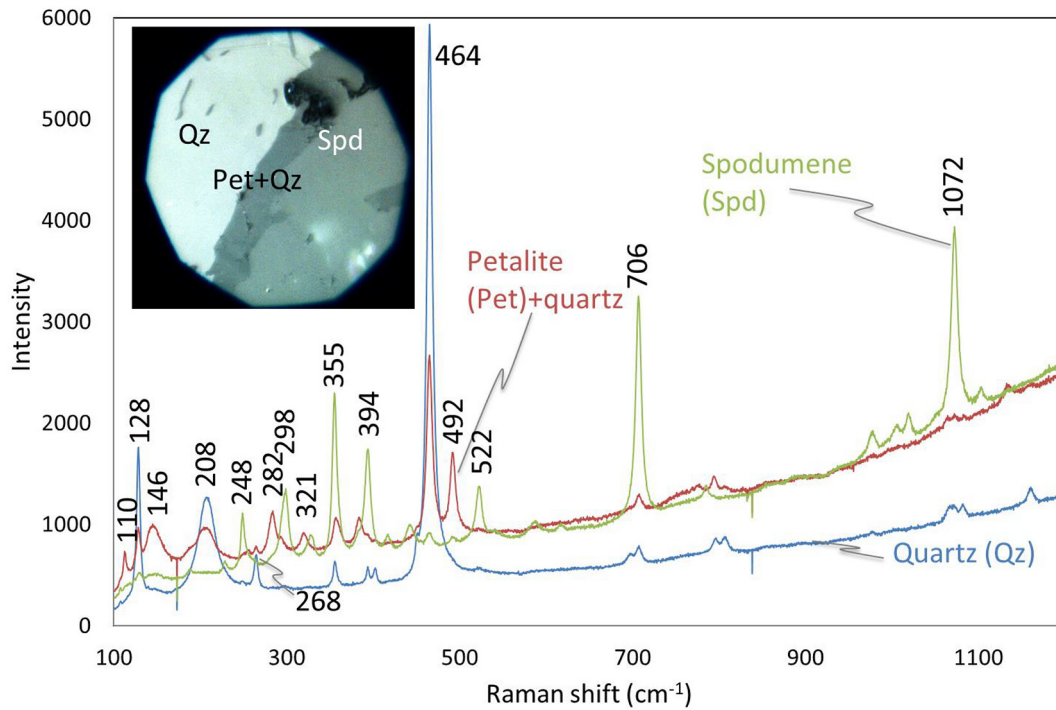
Fig. 9. Raman spectra of quartz (Qz), spodumene (Spd) and petalite + quartz (Pet+Qz) obtained across the reaction zone shown in the reflected light image in the inset (quartz – bright, petalite + quartz – dark grey, spodumene – medium grey).

Table 3
^{40}Ar/^{39}Ar age data for muscovite from the spodumene pegmatite.

| T °C	cc stp ^{39}Ar	% ^{39}Ar	Included	Age Ma ± 95%	Ca/K ± 95%	Cl/K ± 95%
500	5.3E-12	0.36	no	1178.8 ± 33.9	–	0.0087 ± 0.0010
570	1.194E-11	0.81	no	1854.5 ± 16.9	–	0.0016 ± 0.0002
640	4.115E-11	2.78	no	1990.8 ± 10.0	–	0.0014 ± 0.0002
710	1.029E-10	6.94	yes	2012.8 ± 9.4	–	0.0016 ± 0.0002
780	2.36E-10	15.92	yes	2020.7 ± 8.5	–	0.0015 ± 0.0002
850	3.589E-10	24.21	yes	2023.6 ± 7.8	–	0.0015 ± 0.0002
920	3.071E-10	20.72	yes	2030.6 ± 8.0	–	0.0015 ± 0.0002
990	5.843E-11	3.94	yes	2030.9 ± 10.4	–	0.0015 ± 0.0002
1060	1.27E-10	8.57	yes	2036.4 ± 10.5	–	0.0015 ± 0.0002
1130	4.618E-11	3.12	yes	2032.1 ± 11.0	–	0.0015 ± 0.0002
1200	4.832E-11	3.26	yes	2038.2 ± 9.3	–	0.0014 ± 0.0002
1270	8.427E-11	5.69	yes	2030.7 ± 10.0	–	0.0015 ± 0.0002
1340	5.338E-11	3.60	yes	2041.8 ± 9.5	–	0.0016 ± 0.0002
1400	1.366E-12	0.09	no	2081.9 ± 63.4	–	0.0014 ± 0.0010
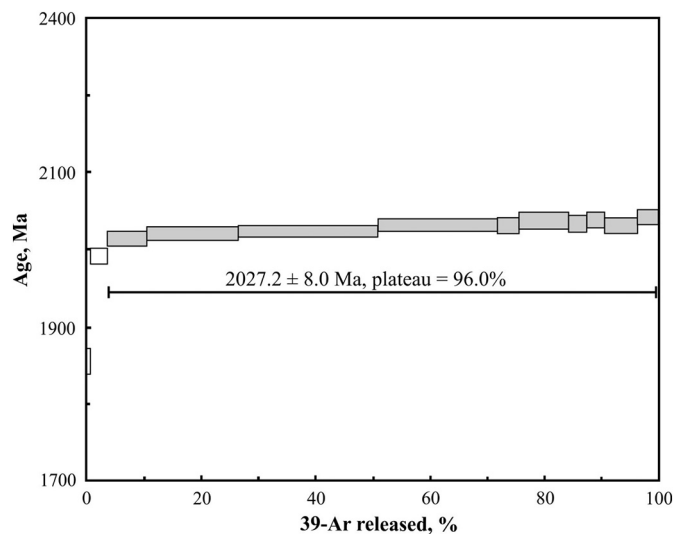
Fig. 10. ^{40}Ar/^{39}Ar age spectra for muscovite from the spodumene pegmatite.

the time of the last strong thermal event. Hence, we interpret the ~2.02 Ga ^{40}Ar/^{39}Ar age as the timing of effect of the meteorite impact on the spodumene pegmatites.

9. Discussion

9.1. Formation of petalite postdates the subsolidus stage in the pegmatite

Petalite reaction zones typically follow the spodumene grain margins at their contacts with quartz in the Vredefort granitic pegmatite (Fig. 11). The textural relation of spodumene and quartz invading each other, and the occurrence of petalite around spodumene (Figs. 7a to c and 11), are interpreted to indicate the reaction.

$$spodumene + 2\ quartz = petalite \tag{1}$$

However, this textural relation is not unambiguous.

For example, petalite is associated with vermicular spodumene-quartz intergrowths (Fig. 7d). This texture is comparable to the symplectic spodumene-quartz intergrowths (SQIs) commonly reported
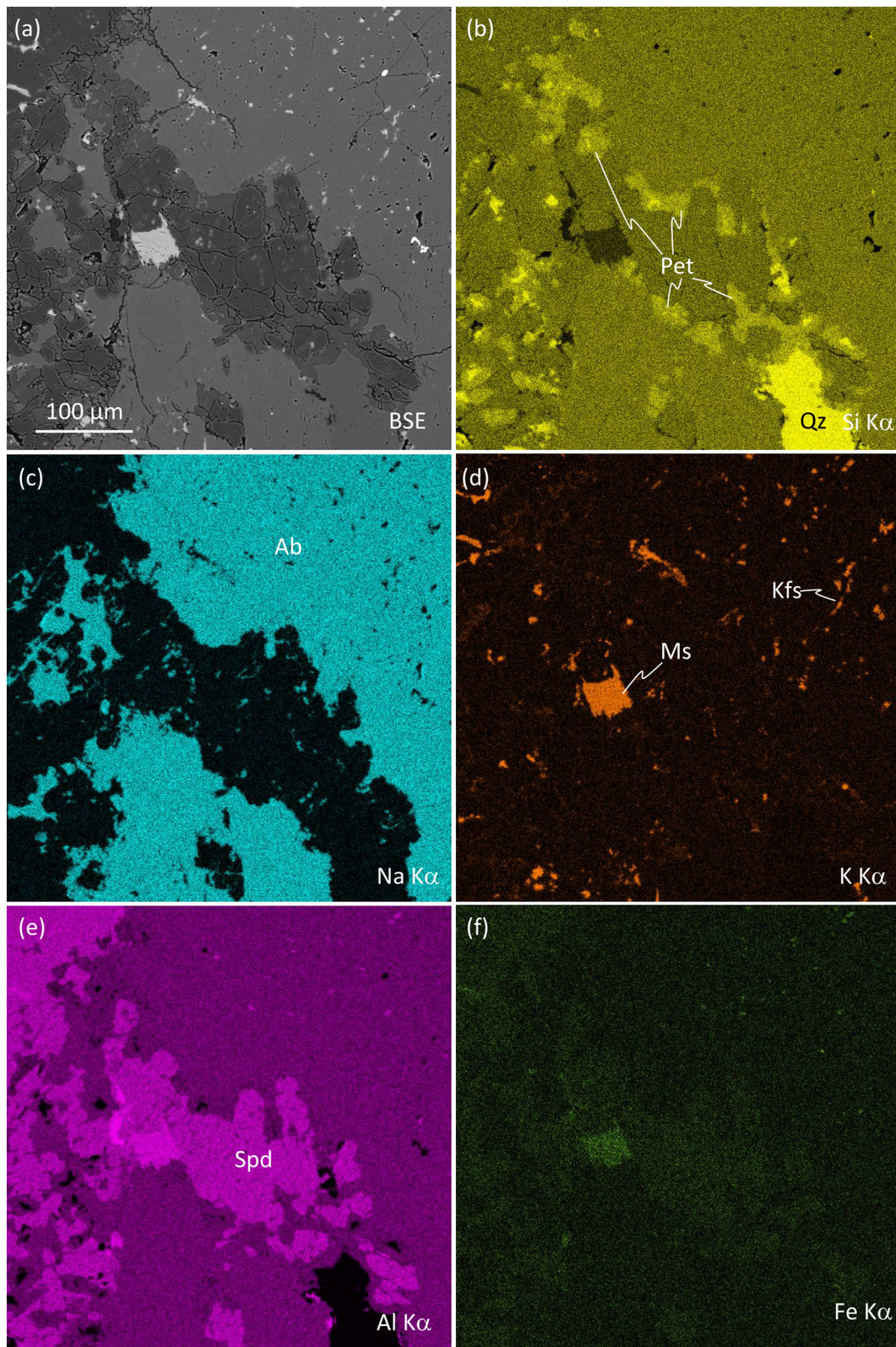
Fig. 11. EDS elemental mapping of a representative rock domain involving spodumene, quartz, petalite, albite, muscovite and K-feldspar. (**a**) BSE image, (**b**) Si Kα, (**c**) Na Kα, (**d**) K Kα, (**e**) Al Kα, (**f**) Fe Kα. The petalite rims conspicuously follow the margin of spodumene. Note that the muscovite is separated from petalite by spodumene [better seen in (b)].

from lithium-rich granitic pegmatites and interpreted as pseudomorphic replacement of petalite via reverse reaction (1) (Černý and Ferguson, 1972; Chakoumakos and Lumpkin, 1990; London and Burt, 1982; Thomas et al., 1993). For example, in the Tanco pegmatite,

Manitoba, Canada, large petalite crystals are frequently penetrated by fine-grained symplectites of spodumene and quartz, and by coarse aggregates of parallel spodumene fibres embedded in quartz (Černý and Ferguson, 1972). In the Highburg pegmatite, Natal Belt, southern

Africa, spodumene occurs as part of centimeter-scale graphic and symplectic intergrowths with quartz, which constitute up to 70% of the rock (Thomas et al., 1993). In these studies, the bulk composition of the spodumene-quartz intergrowth is close to that of petalite. Together with the textural evidence, they argued for the formation of spodumene-quartz intergrowths by the breakdown of petalite (Černý and Ferguson, 1972; Thomas et al., 1993). Unlike these studies, the spodumene-quartz intergrowth documented in the present study is localized in occurrence. No such textures are seen in the large spodumene crystals from the pegmatite and no remnants of primary petalite occur in the pegmatite. The modal proportion of spodumene:quartz in the intergrowth (e.g., Fig. 7d) indicates a ratio of ~81:19, which is different from the ~60:40 ratio reported for spodumene-quartz intergrowths by Thomas et al. (1993). In the common case, spodumene resulting from the breakdown of former magmatic petalite shows a low iron content (Černý and Ferguson, 1972; Thomas et al., 1993). This is different from those reported for spodumene in this study. Thus, the localized occurrence of the spodumene-quartz intergrowths in the Vredefort pegmatite is not evidence for earlier petalite.

Charoy et al. (2001) reported thin petalite rims on spodumene in lithium-rich granitic pegmatites from northern Portugal. This texture is comparable to that observed in the present study (Figs. 7 and 11). However, Charoy et al. (2001) documented that spodumene is locally penetrated but not replaced by petalite along cracks or twin planes. They also reported needles of petalite, together with euhedral quartz, filling angular voids among a meshwork of euhedral laths of spodumene (see Charoy et al., 2001). Importantly, spodumene is replaced by albite ($\pm$ muscovite), while petalite is altered to eucryptite and K-feldspar during the subsolidus stage via interaction with a residual magmatic fluid (Charoy et al., 2001). Unlike this scenario, the petalite + quartz reaction zones in the studied pegmatites do not show any subsolidus K-feldspar, which is prevalent in spodumene and albite (see Figs. 6, 7 and 11). This clearly indicates that the formation of petalite postdates the subsolidus evolution stage of the pegmatite and is not related to interaction with a fluid.

9.2. Likely conditions and geological scenario for the formation of petalite

In the quartz-saturated conditions characteristic for granitic pegmatites, phase relations between the lithium aluminosilicates are a function of temperature and pressure and are largely independent on the proportions of other phases (Krivovichev, 2004; London, 1984; Stewart, 1978). The pressure and temperature conditions of formation of spodumene and petalite can be roughly estimated from the lithium aluminosilicate phase diagram (Fig. 1; London, 1984). Pegmatites in which spodumene is the primary lithium aluminosilicate are constrained to begin crystallization at about 650 °C and ~3–5 kbar and reach solidus at 500–550 °C (Černý, 1991; Chakoumakos and Lumpkin, 1990; London, 1984). Thus, the formation of petalite via reaction (1) in the subsolidus occurred below this temperature and, following Fig. 1, required either an increase in temperature or a decrease in pressure (London, 1984; Stewart, 1978). A combination of two processes cannot be excluded, as well. There are two nearly coeval events, which could provide heating and/or decrease of pressure after a complete solidification of the rock: the ~2.06–2.05 Ga Bushveld magmatic event and the ~2.02 Ga Vredefort impact event.

The ~2.06–2.05 Ga Bushveld magmatic event including the Bushveld Complex and Molopo Farms Complex layered intrusions (Fig. 2a) is one of the largest intracratonic large igneous provinces in the world (see Rajesh et al., 2013 and references therein; Ernst, 2014). Different studies pointed out the heat and fluid effects related to the Bushveld magmatic event to regions in and around the Vredefort impact structure (Friese et al., 2003; Gibson et al., 2000; Rasmussen et al., 2007; Robb et al., 1997). ~2.06 to 2.04 Ga [40]Ar/[39]Ar mica-amphibole overprint ages have been reported from the region (Allsopp et al., 1991; Friese et al., 2003; Gibson et al., 2000). Estimates of the duration of elevated geothermal

gradients in the region indicate that the generation and migration of hot fluids were sustained for at least ~20 Ma (Gibson and Stevens, 1998). A number of *syn*-Bushveld intrusions occur in the northern part of the Vredefort impact structure (Bisschoff, 1972; Coetzee et al., 2006; De Waal et al., 2006, 2008; Graham et al., 2005). However, these bodies are essentially restricted to the northern collar of the Vredefort structure. No syn-Bushveld intrusion is reported from the southeastern sector, including the Greenlands granite-greenstone complex (Colliston and Reimold, 1990; Hart et al., 2004; Lana et al., 2003; Minnitt et al., 1994; Reimold et al., 1988). Importantly, the ~2.02 Ga [40]Ar/[30]Ar muscovite age reported in this study is closer to the meteorite impact age. Hence, discarding the possibility of effect of the Bushveld event, the next event to consider is the ~2.02 Ga meteorite impact, which in general, is able to provide both heat and decompression.

The decompression scenario for the formation of the petalite rims is justified by the location of the pegmatite body near the "uplifted central core" of the Vredefort structure, which experienced the post-impact uplift. However, in this case, the petalite textures must be formed within the whole pegmatite body, not only locally near the pseudotachylite veins. For this reason, the decompression is hardly to be a leading factor in the petalite-forming reaction. Thus, the only process suitable for the formation of the petalite textures is post-impact heating. The relations between the petalite textures and rock-forming minerals allow for specification of the extent of this process.

The EDS elemental (Si, Na, K, Al, Fe) maps in Fig. 12a to f show that petalite occurs not only between spodumene and albite, but also at the interface of muscovite and quartz. However, muscovite has smooth regular (near straight-line) grain margins with petalite, while the contact between spodumene and petalite is irregular and lobate. Petalite $\pm$ quartz conspicuously follows the grain margins of spodumene (Fig. 12). Fig. 13a to f show that petalite is restricted to spodumene grain boundaries and does not form along muscovite or albite interfaces. The restricted development of petalite is also seen in Fig. 11, where it is separated from muscovite by spodumene. K-feldspar is not associated with the petalite textures. No textures indicating decomposition of muscovite to form K-feldspar are present in the rock. All the above relations indicate that muscovite did not participate in the petalite formation, which proceeded within the muscovite + quartz P-T stability field (see Fig. 1), and thus, did not exceed 550–600 °C.

9.3. Role of the meteorite impact in the formation of petalite – A unique geological scenario

The Vredefort spodumene pegmatites are unique in terms of their occurrence within a meteorite impact structure. Shock metamorphism is known to generate high temperatures and pressures in the target rocks (Melosh, 1989). The latter is manifested in shock deformational features exposed within the impact structure. Depending on the distance from the central core, rocks from different parts of the Vredefort impact structure variably preserve macroscopic field features including pseudotachylites, shatter cones and overturned beds. Documented micro-deformation features include planar deformation features (PDFs) in quartz (e.g., Grieve et al., 1990; Kovaleva et al., 2018; Leroux et al., 1994), zircon (e.g., Graham et al., 2005; Kamo et al., 1996; Moser et al., 2011; Reimold et al., 2002), monazite (Flowers et al., 2003), recrystallized diaplectic glass and shock melts in feldspars (Gibson and Reimold, 2005) and the occurrence of checkerboard feldspar (Buchanan and Reimold, 2002). Minerals newly formed during the impact are rarely reported from the Vredefort impact structure. Granular zircon neoblasts still retaining the original morphology of the grains have been reported (e.g., Kamo et al., 1996; Moser, 1997). High-pressure SiO_2 polymorphs, coesite and stishovite, are found in pseudotachylites from the collar rocks (Martini, 1991).

Petalite overgrowths in spodumene pegmatites can be a new mineral formed by the meteorite impact. This interpretation is supported
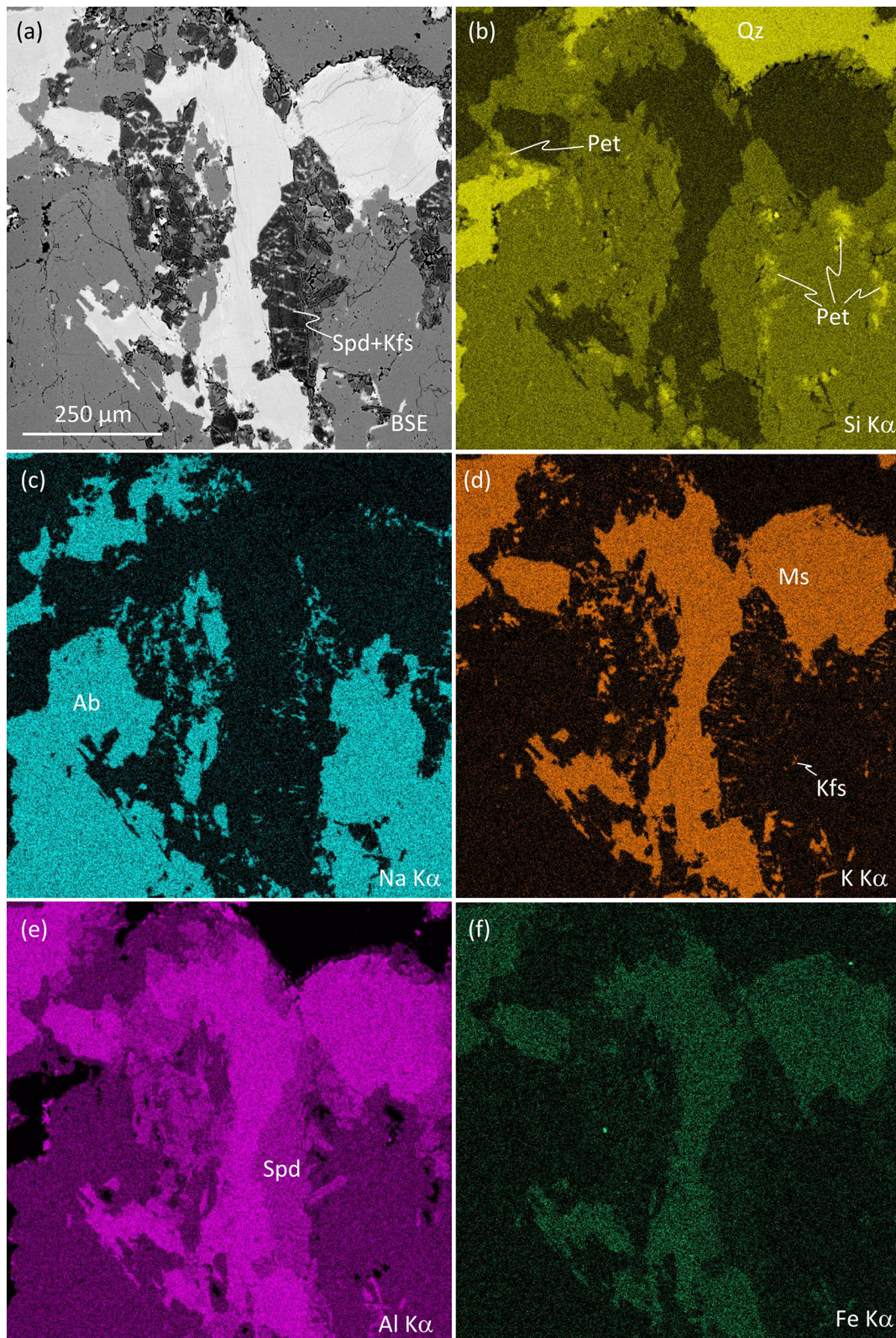
Fig. 12. EDS elemental mapping of a representative rock domain involving spodumene, quartz, petalite, albite, muscovite and K-feldspar. (**a**) BSE image, (**b**) Si Kα, (**c**) Na Kα, (**d**) K Kα, (**e**) Al Kα, (**f**) Fe Kα. Petalite occurs at the interface of muscovite and quartz [see upper left quadrant; better seen in (b)]. The contact of muscovite with petalite is smooth regular (near straight-line). This is different to the irregular-lobate grain margin between spodumene and petalite.

by field observations of impact-related pseudotachylite veins (Fig. 5) cutting across the pegmatites. Petalite rims are restricted to pegmatite sampled closer to the pseudotachylite veins. The angular fragments within the pseudotachylite veins cutting across the spodumene pegmatites indicate that they were shaken and broken but were not stirred and moved by the cataclastic process (e.g., Garde and Klausen, 2016).
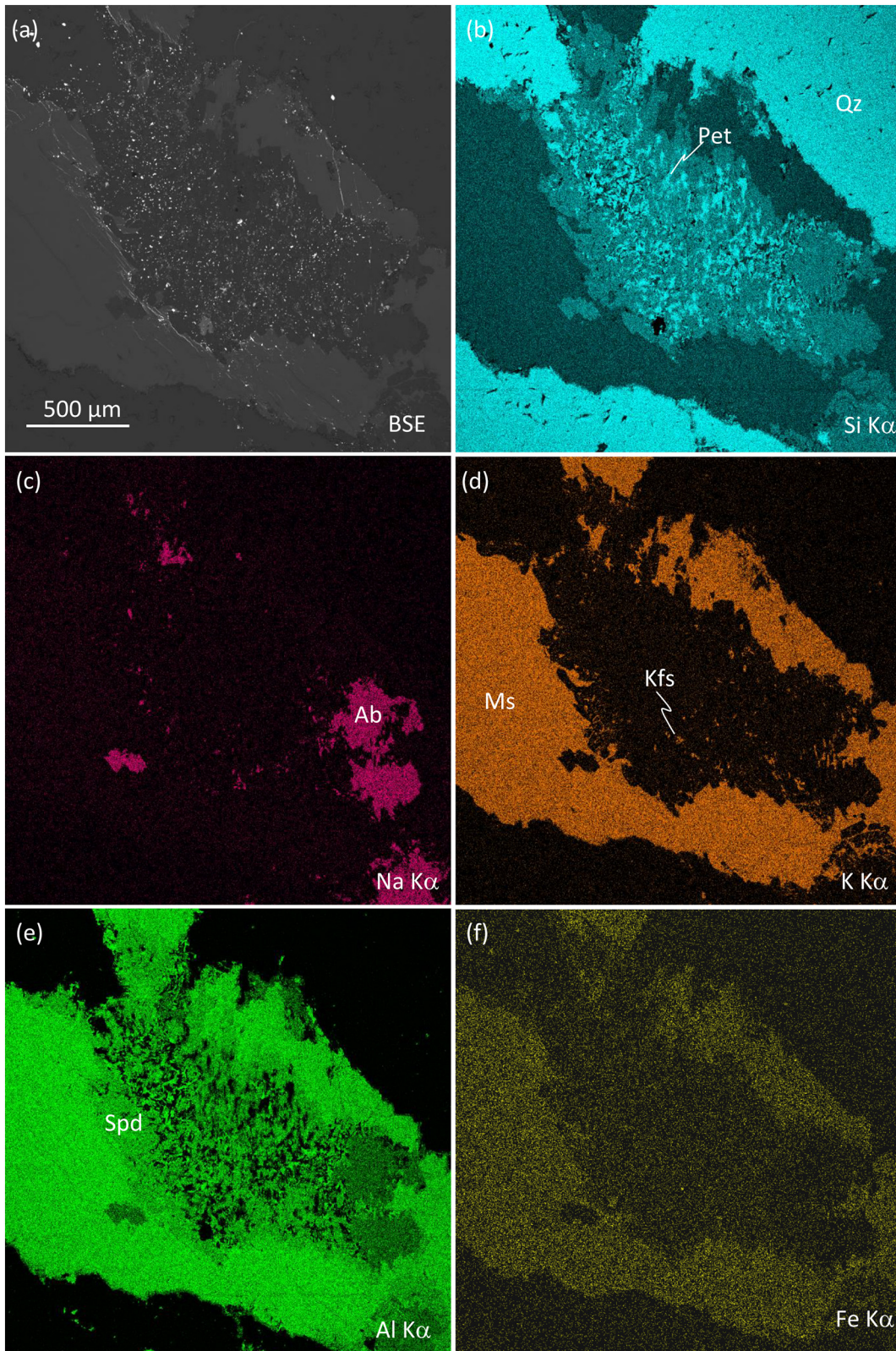
Fig. 13. EDS elemental mapping of a representative rock domain involving spodumene, quartz, petalite, albite, muscovite and K-feldspar. (**a**) BSE image, (**b**) Si Kα, (**c**) Na Kα, (**d**) K Kα, (**e**) Al Kα, (**f**) Fe Kα. Petalite is restricted to spodumene and quartz and does not occur along the interface of muscovite or albite.

The later which are primarily related to the original impact would have resulted in rounded grains as seen elsewhere in the Vredefort impact structure. The distance from the central uplift of the impact structure also likely played a role in this. This argues for a prominence of post-shock effect on the spodumene pegmatite in the southeastern part of the impact structure.

Based on metamorphic assemblages in rocks from different parts of the impact structure, Gibson and Reimold (2008) estimated post-shock temperatures of >1000 °C from the inner core to 700–1000 °C for the outer core (see inset in Fig. 3). The temperature progressively decreases through the intermediate zone with 500–700 °C to 400–500 °C and < 400 °C in the outer zones (see inset in Fig. 3). The spodumene pegmatites occur outside the central most portion of the impact structure where very high temperatures are reported. They are exposed within the intermediate zone, where post-shock temperatures of 500–700 °C were estimated. This temperature is enough to form petalite from spodumene and quartz (Fig. 1). BSE-SEM imaging did not delineate any features similar to PDFs in quartz from the spodumene pegmatites and this is probably due to the strong annealing by the post-impact metamorphism. Raman analyses of quartz adjacent to spodumene and petalite did not show peaks for coesite or stishovite. The restricted distribution of high pressure silica polymorphs in the Vredefort impact structure have been attributed to post-shock thermal effects, which may have destroyed these minerals throughout much of the impact structure (e.g., Martini, 1991).

Thus, a unique scenario to achieve the condition for the formation of petalite in a granitic pegmatite likely involves high temperatures generated in the target rocks by post-shock thermal event related to the ~2.02 Ga meteorite impact.

10. Concluding remarks

Meteorite impact structures continue to surprise us with the amount of geologic information preserved in the rocks exposed within them. As the rocks within impact structures are variably overprinted by shock and post-shock deformational and/or thermal metamorphic features, phase transition of minerals is expected. The most commonly reported include the formation of high-pressure polymorphs of silica, coesite, and stishovite (Melosh, 1989). The extreme P-T conditions achieved during shock and post-shock events could result in the formation of extremely rare minerals, whose natural occurrence is scarce and which are often produced in the laboratory. For example, reidite, a high-pressure polymorph of zircon, was reported in sandstone from the ~470–450 Ma Rock Elm meteorite impact structure in North America (Cavosie, 2015). The extreme conditions can also result in rare scenarios such as in the present study where petalite formed in the intermediate zone of the ~2.02 Ga Vredefort impact structure. The spodumene pegmatites were at the right place at the right time to be affected by heating to form petalite after its subsolidus evolution stage. The identification of reidite (Cavosie, 2015) and petalite (this study), from target rocks, one porous and the other crystalline, respectively, raises the possibility that other minerals, especially rare phases, formed at extreme P-T conditions and under rare circumstances such as after the subsolidus stage can be found in nature.

Declaration of Competing Interest

None.

Acknowledgments

Appendix A. Supplementary data

References

Allsopp, H.L., Fitch, F.J., Miller, J.A., Reimold, W.U., 1991. ^{40}Ar/^{39}Ar stepheating age determinations relevant to the formation of the Vredefort Dome, South Africa. S. Afr. J. Sci. 87, 431–442.

Antoine, L.A.G., Nicolaysen, L.O., Nicol, S.L., 1990. Processed and enhanced gravity and magnetic images over the Vredefort structure and their interpretation. Tectonophysics 171, 63–74.

Armstrong, R.A., Lana, C., Reimold, W.U., Gibson, R.L., 2006. SHRIMP zircon age constraints on Mesoarchean crustal development in the Vredefort dome, central Kaapvaal craton, South Africa. In: Reimold, W.U., Gibson, R.L. (Eds.), Processes on the Early Earth. 405. Geological Society of America, Special Paper, pp. 233–253.

Benaway, R., Sirbescu, M.-L.C., Schmidt, C., 2012. Evaluation of water-rich boundary layers formed during partial crystallization of synthetic pegmatite melts. Geol. Soc. Am. Abstr. Programs 44 (7), 249.

Bisschoff, A.A., 1972. Tholeiitic intrusions in the Vredefort Dome. Trans. Geol. Soc. S.A. 75, 23–30.

Bisschoff, I., Bisschoff, A.A., 1988. A lithium-bearing pegmatite from the Vredefort dome. S. Afr. J. Geol. 91, 550–552.

Buchanan, P.C., Reimold, W.U., 2002. Planar deformation features and impact glass in inclusions from the Vredefort Granophyre, South Africa. Meteorit. Planet. Sci. 37, 807–822.

Cavosie, A., 2015. Nanoscale records of ancient shock deformation: Reidite (ZrSiO$_4$) in sandstone at the Ordovician Rock Elm impact crater. Geology 43 (4), 315–318.

Černý, P., 1991. Rare-element granite pegmatites. Part I: anatomy and internal evolution of pegmatite deposits. Geosci. Can. 18, 49–67.

Černý, P., Ercit, T.S., 2005. The classification of granitic pegmatites revisited. Can. Mineral. 43, 2005–2026.

Černý, P., Ferguson, R.B., 1972. The Tanco Pegmatite at Bernic Lake, Manitoba. IV. Petalite and spodumene relations. Can. Mineral. 11, 660–678.

Chakoumakos, B.C., Lumpkin, G.R., 1990. Pressure–temperature constraints on the crystallization of the Harding pegmatite, Taos County, New Mexico. Can. Mineral. 28, 287–298.

Charoy, B., Noronha, F., Lima, A., 2001. Spodumene–petalite–eucryptite: Mutual relationships and pattern of alteration in Li-rich aplite–pegmatite dykes from northern Portugal. Can. Mineral. 39, 729–746.

Coetzee, M.S., Beukes, G.J., de Bruiyn, H., Bisschoff, A.A., 2006. Geochemistry and petrogenesis of tholeiitic intrusions of possible Bushveld-age in the Vredefort Dome, South Africa. J. Afr. Earth Sci. 45, 213–235.

Colliston, W.P., Reimold, W.U., 1990. Structural studies in the Vredefort Dome; preliminary interpretations of results on the southern portion of the structure. Economic Geology Research Unit Information Circular. 229. University of the Witwatersrand, Johannesburg, South Africa, p. 42.

De Waal, S.A., Graham, I.T., Armstrong, R.A., 2006. The Lindeques Drift and Heidelberg intrusions and the Roodekraal complex, Vredefort, South Africa: Comagmatic plutonic and volcanic products of a 2055 Ma ferrobasaltic magma. S. Afr. J. Geol. 109, 279–300.

De Waal, S.A., Schweitzer, J., Graham, I.T., Gauert, T., Ripley, E., 2008. A Bushveld-related high-Ti igneous suite HITIS derived from an alkali to transitional basaltic magma, South Africa. S. Afr. J. Geol. 111, 201–224.

Ernst, R., 2014. Large igneous provinces. Cambridge University Press, p. 653.

Flowers, R.M., Moser, D.E., Hart, R.J., 2003. Evolution of the amphibolite-granulite facies transition exposed by the Vredefort impact structure, Kaapvaal Craton, South Africa. J. Geol. 111, 455–470.

French, B.M., Jazek, P.A., Appleman, D.E., 1978. Virgilite, a new lithium aluminum silicate mineral from the Macusani glass, Peru. Am. Mineral. 63, 461–465.

Friese, A.W., Reimold, W.U., Layer, P.W., 2003. ^{40}Ar-^{39}Ar dating of and structural information on tectonite-bearing faults in the Witwatersrand Basin: evidence for multi-stage, tectono-thermal activity in the central Kaapvaal Craton. S. Afr. J. Geol. 106, 41–70.

Garde, A.A., Klausen, M.B., 2016. A centennial reappraisal of the Vredefort pseudotachylytes: shaken, not stirred by meteorite impact. J. Geol. Soc. Lond. 173 (6), 954–965.

Gibson, R.L., Reimold, W.U., 2005. Shock pressure distribution in the Vredefort impact structure, South Africa. Geol. Soc. Am. Spec. Pap. 384, 329–349.

Gibson, R.L., Reimold, W.U., 2008. Geology of the Vredefort Impact Structure, a Guide to Sites of Interest. 97. Council of Geoscience, Pretoria, Memoir, p. 181.

Gibson, R.L., Stevens, G., 1998. Regional metamorphism due to anorogenic intracratonic magmatism. In: Treloar, P.J., O'Brien, P. (Eds.), What Drives Metamorphism and Metamorphic Reactions?. 138. Geological Society, London, Special Publication, pp. 121–135.

Gibson, R.L., Reimold, W.U., Phillips, D., Layer, P.W., 2000. ^{40}Ar/^{39}Ar constraints on the age of metamorphism in the Witwatersrand Supergroup, Vredefort dome (South Africa). S. Afr. J. Geol. 103, 175–190.

Graham, I.T., De Waal, S.A., Armstrong, R.A., 2005. New U–Pb SHRIMP zircon age for the Schurwedraai alkali granite: Implications for pre-impact development of the

Vredefort Dome and extent of Bushveld magmatism, South Africa. J. Afr. Earth Sci. 43, 537–548.

Grieve, R.A.F., Coderre, J.M., Robertson, P.B., Alexopoulos, J., 1990. Microscopic planar deformation features in quartz of the Vredefort structure: Anomalous but still suggestive of an impact origin. Tectonophysics 171, 185–200.

Harrison, T.M., Célérier, J., Aikman, A.B., Hermann, J., HeizLer, M.T., 2009. Diffusion of ^{40}Ar in muscovite. Geochim. Cosmochim. Acta 73, 1039–1051.

Hart, R.J., Moser, D., Andreoli, M.A.G., 1999. Archaean age for the granulite facies metamorphism near the Centre of the Vredefort Structure, South Africa. Geology 27 (12), 1091–1094.

Hart, J.H., McDonald, I., Tredoux, M., de Witt, M.J., Carlson, R.W., Andreoli, A., Moser, D.E., Ashwal, L.D., 2004. New PGE and Re/Os-isotope data from lower crustal sections of the Vredefort Dome and reinterpretation of its "crust on edge" profile. S. Afr. J. Geol. 107, 173–184.

Kamo, S.L., Reimold, W.U., Krogh, T.E., Colliston, W.P., 1996. A 2.023 Ga age for the Vredefort impact event and a first report of shock metamorphosed zircons in pseudotachylitic breccias and granophyres. Earth Planet. Sci. Lett. 144 (3–4), 369–387.

Kerrick, D.M., 1972. Experimental determination of muscovite + quartz stability with P (H$_2$O) < P(total). Am. J. Sci. 272, 946–958.

Kovaleva, E., Huber, M.S., Roelofse, F., Tredoux, M., Praekelt, H., 2018. Pseudotachylite vein hosted by a clast in the Vredefort Granophyre: characterization, origin and relevance. S. Afr. J. Geol. 121 (1), 51–68.

Krivovichev, V.G., 2004. Mineral equilibria with spodumene, petalite and eucryptite. I. System Li$_2$O–Al$_2$O$_3$–SiO$_2$–H$_2$O—thermodynamical analysis and geological application. Proceed. Russian Mineral. Soc. 133 (1), 23–31.

Lagache, M., Dujon, S.C., Sebastian, S., 1995. Assemblages of Li–Cs pegmatite minerals in equilibrium with a fluid from their primary crystallization until their hydrothermal alteration: an experimental study. Mineral. Petrol. 55, 131–143.

Lana, C., Gibson, R.L., Reimold, W.U., Minnitt, R.A.M., 2003. Geology and geochemistry of a granite-greenstone association in the southeastern Vredefort dome, South Africa. S. Afr. J. Geol. 106, 291–314.

Lana, C., Gibson, R.L., Reimold, W.U., 2006. The Broodkop shear zone, southeast Vredefort dome (South Africa): a Dominion-related extensional feature? S. Afr. J. Geol. 109, 265–278.

Leroux, H., Reimold, W.U., Doukhan, J.C., 1994. A TEM investigation of shock metamorphism in quartz from the Vredefort dome, South Africa. Tectonophysics 230, 223–239.

London, D., 1984. Experimental phase equilibria in the system LiAlSiO$_4$–SiO$_2$–H$_2$O: a petrogenetic grid for lithium-rich pegmatites. Am. Mineral. 69, 995–1004.

London, D., 2008. Pegmatites. Canadian Mineralogist. 10. Special Publication, p. 368.

London, D., Burt, D.M., 1982. Alteration of spodumene, montebrasite and lithiophilite in pegmatites of the White Picacho district, Arizona. Am. Mineral. 67, 97–113.

Martini, J.E.J., 1991. The nature, distribution and genesis of the coesite and stishovite associated with pseudotachylite of the Vredefort Dome, South Africa. Earth Planet. Sci. Lett. 103, 285–300.

McCarthy, T.S., Corner, B., Lombard, H., Beukes, N.J., Armstrong, R.A., Cawthorn, R.G., 2018. The pre-Karoo geology of the southern portion of the Kaapvaal Craton, South Africa. S. Afr. J. Geol. 121 (1), 1–22.

Melosh, H.J., 1989. Impact Cratering—A Geologic Process. Oxford University Press, New York, p. 245.

Minnitt, R.C.A., Reimold, W.U., Colliston, W.P., 1994. The geology of the Greenlands Greenstone complex and selected granitoid terranes in the south-eastern quadrant of the Vredefort Dome. Economic Geology Research Unit Information Circular. 281. University of Witwatersrand, Johannesburg, South Africa, p. 46.

Monier, G., Robert, J.L., 1986. Evolution of the miscibility gap between muscovite and biotite solid solutions with increasing lithium content: an experimental study in the system K$_2$O–Li$_2$O–MgO–FeO–Al$_2$O$_3$–SiO$_2$–H$_2$O–HF at 600°C, 2 kbar P$_{H2O}$: comparison with natural lithium micas. Mineral. Mag. 50, 641–651.

Moser, D.E., 1997. Dating the shock wave and thermal imprint of the giant Vredefort impact, South Africa. Geology 25, 7–10.

Moser, D.E., Flowers, R.M., Hart, R.J., 2001. Birth of the Kaapvaal Tectosphere 3.08 billion years ago. Science 291, 465–468.

Moser, D.E., Cupelli, C.L., Barker, I.R., Flowers, R.M., Bowman, J.R., Wooden, J., Hart, J.R., 2011. New zircon shock phenomena and their use for dating and reconstruction of

large impact structures revealed by electron nanobeam (EBSD, CL, EDS) and isotopic U-Pb and (U-Th)/He analysis of the Vredefort dome. Can. J. Earth Sci. 48 (2), 117–139.

Pommier, C.J.S., Denton, M.B., Downs, R.T., 2003. Raman spectroscopic study of spodumene (LiAlSi$_2$O$_6$) through the pressure-induced phase change from C2/c to P2 1 /c. J. Raman Spectrosc. 34, 769–775.

Pybus, G.Q.J., 1995. Geological and mineralogical analysis of some mafic intrusions in the Vredefort Dome, Central Witwatersrand Basin. MSc Thesis (unpublished). Univ. of the Witwatersrand, Johannesburg, p. 376.

Rajesh, H.M., Knoper, M.W., 2012. Discussion of "New zircon shock phenomena and their use for dating and reconstruction of large impact structures revealed by electron nanobeam (EBSD, CL, EDS) and isotopic U-Pb and (U-Th)/He analysis of the Vredefort dome". Can. J. Earth Sci. 49, 857–862.

Rajesh, H.M., Chisonga, B.C., Shindo, K., Beukes, N.J., Armstrong, R.A., 2013. Petrographic, geochemical and SHRIMP U-Pb titanite age characterization of the Thabazimbi mafic sills: Extended time frame and a unifying petrogenetic model for the Bushveld large Igneous Province. Precambrian Res. 230, 79–102.

Rasmussen, B., Fletcher, I.R., Muhling, J.R., Mueller, A.G., Hall, G.C., 2007. Bushveld-aged fluid flow, peak metamorphism, and gold mobilization in the Witwatersrand basin, South Africa: constraints from in situ SHRIMP UP-b dating of monazite and xenotime. Geology 35, 931–934.

Reimold, W.U., Colliston, W.P., 1994. Pseudotachylites of the Vredefort Dome and the surrounding Witwatersrand Basin, South Africa. In: Dressler, B.O., Grieve, R.A.F., Sharpton, V.L. (Eds.), Large Meteorite Impacts and Planetary Evolution. Geological Society of America Special Paper. 293. Colorado, Boulder, pp. 177–196.

Reimold, W.U., Colliston, W.P., Robertson, A.S., 1988. Chronological and structural work in the Vredefort Dome. Extended Abstracts, Geocongress. 88. Geological Society of South Africa, Durban, South Africa, pp. 501–504.

Reimold, W.U., Pybus, G.Q.J., Kruger, F.J., Layer, P.W., Koeberl, C., 2000. The Anna's Rust Sheet and related gabbroic intrusions in the Vredefort Dome – Kibaran magmatic event on the Kaapvaal Craton and beyond? J. Afr. Earth Sci. 31 (3–4), 499–521.

Reimold, W.U., Leroux, H., Gibson, R.L., 2002. Shocked and thermally metamorphosed zircon from the Vredefort impact structure, South Africa: a transmission electron microscopic study. Eur. J. Mineral. 14, 859–868.

Robb, L.J., Charlesworth, E.G., Drennan, G.R., Gibson, R.L., Tongu, E.L., 1997. Tectonometamorphic setting and paragenetic sequence of Au-U mineralisation in the Archaean Witwatersrand Basin, South Africa. Aust. J. Earth Sci. 44, 353–371.

Robertson, A.S., 1988. U-Pb isotope analysis of selected lithologies from the Broodkop migmatite complex, South-Eastern Vredefort Dome. Unpublished B.Sc. Honours Dissertation. University of the Witwatersrand, Johannesburg, South Africa, p. 84.

Sirbescu, M.C., Schmidt, C., Veksler, I.V., Whittington, A.G., Wilke, M., 2017. Experimental Crystallization of Undercooled Felsic Liquids: Generation of Pegmatitic Texture. J. Petrol. 58, 539–568.

Stangarone, C., Prencipe, M., Mantovani, L., Bersani, D., Tribaudino, M., Lottici, P.P., 2014. Ab initio calculated and experimentally measured Raman spectra of spodumene (LiAlSi$_2$O$_6$). Abstract volume of 11th GeoRaman International Conference, 2014, Missourri, USA, p. 5061.

Stewart, D.B., 1978. Petrogenesis of lithium-rich pegmatites. Am. Mineral. 63, 970–980.

Tagai, T., Ried, H., Joswig, W., Korekawa, M., 1982. Kristallographische Untersuchungen eines Petalits mittels Neutronenbeugung und Transmissionselektroneomikroskopie. Zeitschrift fUr Kristallographie 160, 159–170.

Thomas, R.J., Buhmann, D., Bullen, W.D., Scogings, A.J., Bruin, D.De., 1993. Unusual spodumene pegmatites from the late Kibaran of southern Natal, South Africa. Ore Geol. Rev. 9, 161–182.

Tindle, A.G., Webb, P.C., 1990. Estimation of lithium contents in trioctahedral micas using microprobe data; application to micas from granitic rocks. Eur. J. Mineral. 2 (5), 595–610.

Tischendorf, G., Gottesmann, B., Förster, H.J., Trumbull, R.B., 1997. On Li-bearing micas: estimating Li from electron microprobe analyses and improved diagram for graphical representation. Mineral. Mag. 61 (6), 809–834.

Wood, S.A., Williams-Jones, A.E., 1993. Theoretical studies of the alteration of spodumene, petalite, eucryptite and pollucite in granitic pegmatites: exchange reactions with alkali feldspars. Contrib. Mineral. Petrol. 114, 255–263.